01 Jan 2023

Characterization of Virgin, Re-Used, and Oxygen-Reduced Copper Powders Processed by the Plasma Spheroidization Process

M. Hossein Sehhat

David Perez-Palomino

Connor Wiedemeier

Tristan Cullom

et. al. For a complete list of authors, see https://scholarsmine.mst.edu/math_stat_facwork/1143

Recommended Citation

M. Hossein Sehhat et al., "Characterization of Virgin, Re-Used, and Oxygen-Reduced Copper Powders Processed by the Plasma Spheroidization Process," *Advanced Powder Technology*, vol. 34, no. 1, article no. 103885, Elsevier, Jan 2023.
The definitive version is available at https://doi.org/10.1016/j.apt.2022.103885

Advanced Powder Technology 34 (2023) 103885

Contents lists available at ScienceDirect

Advanced Powder Technology

journal homepage: www.elsevier.com/locate/apt

Characterization of Virgin, Re-used, and Oxygen-reduced Copper Powders processed by the Plasma Spheroidization Process

M. Hossein Sehhat [a,*], David Perez-Palomino [a], Connor Wiedemeier [a], Tristan Cullom [b], Joseph W. Newkirk [c]

[a] Department of Mechanical and Aerospace Engineering, Missouri University of Science and Technology, Rolla, MO 65409, United States
[b] Kansas City National Security Campus, Kansas City, MO 64147, United States
[c] Department of Materials Science and Engineering, Missouri University of Science and Technology, Rolla, MO 65409, United States

ARTICLE INFO

Article history:
Received 13 August 2022
Received in revised form 30 October 2022
Accepted 13 November 2022

Keywords:
Additive Manufacturing
Plasma Spheroidization
Sphericity
Copper Powder
Electron Beam Powder Bed Fusion
Oxygen Reduction
Hydrogen Treatment

ABSTRACT

Fabrication of parts with high mechanical properties heavily depend on the quality of powder deployed in the fabrication process. Copper powder in three different powder types were spheroidized using radio-frequency inductively coupled plasma (ICP) spheroidization process (TekSphero-15 system). The characterized powders include virgin powder as purchased from the powder manufacturer, powder used in electron beam powder bed fusion (EB-PBF) process, and reconditioned powder, which was used powder that underwent an oxygen-reduction treatment. The goal of spheroidizing these powder types was to evaluate the change in powder morphology, the possibility of enhancing the powder properties back to their as-received conditions, and assess oxygen reduction of the powder lots given their initial oxygen contents. Also, to investigate the impact of re-spheroidization on powder properties, the second round of spheroidization was performed on the already used-spheroidized powder. The impact of powder type on powder sphericity and particle size distribution was evaluated using the image analysis of scanning electron microscope (SEM) micrographs and laser diffraction, respectively. The spheroidized powder showed higher sphericity and more uniform particle size distribution overall. Depending on the powder collection bin, second round of spheroidization affected the powder sphericity differently. The possibility of deploying the plasma spheroidization process as an alternative oxygen-reduction technique was also investigated through tracking the powders' oxygen content using inert gas fusion method before and after the spheroidization. The plasma spheroidized powder showed less oxygen content than the hydrogen-treated powder. The second round of spheroidization caused no change in oxygen content. The correlation between oxygen-reduction and created cracks was discussed and compared between plasma spheroidization and hydrogen-treatment. The plasma spheroidization process created a powder with higher sphericity, uniform particle size, and less oxygen content.

1. Introduction

Additive Manufacturing (AM) has considerably improved the method of part fabrication in the past few years [1–3]. While several different steps such as machining, welding, and assembling could be performed to fabricate a component using the conventional manufacturing methods, AM can produce the final part in a one-step layer-based process [4–12]. The material feedstock for some of the AM processes is in the form of powder which provides higher flexibility in producing components with high-complex geometries. The powder characteristics, like shape, morphology, and interparticle friction, control the powder performance during such AM processes, especially in terms of powder flowability and spreadability [13], through engaging the particles at their sharp edges which creates large agglomerates [14,15]. Resolving the poor powder performance due to the high cohesivity of fine particles which resulted in agglomeration was studied by Dave et al.

Peer review under responsibility of The copyright line should read:002: Copyright © 2014, The Society of Powder Technology Japan. Published by Elsevier BV and The Society of Powder Technology Japan. All rights reserved..001: Copyright © 2014 Published by Elsevier B.V. on behalf of The Society of Powder Technology Japan. All rights reserved.Please add this footnote for the item group IG000042 "This is the article featuring on ICBMH2019: the 13th International Conference on Bulk Materials Storage, Handling and Transportation.".
* Corresponding author.
E-mail address: hsehhat@mst.edu (M. Hossein Sehhat).

https://doi.org/10.1016/j.apt.2022.103885
0921-8831/

through deploying a milling process and expansion of suspension materials [16–18]. Some techniques like particle coating and surface modification, such as silanization, have been implemented to enhance the flowability of powders since the powder performance can consequently dominate the properties of fabricated parts [19–24]. One of the powder-based AM methods is Electron-Beam Powder Bed Fusion (EB-PBF) process which uses an electron beam to scan powder bed or previously fabricated layer. After fusing and melting the powder particles, each part's layer is solidified, and a new layer of powder is spread for fabrication of next layer [25].

Copper is used for fabrication of parts requiring high electrical and thermal conductivity. Application of copper powder in the EB-PBF process and its related difficulties have been investigated in the literature [26–28]. The copper's high thermal conductivity provides high cooling rates which transfers the heat of melt pool to the powder bed. Since the thermal conductivity of the solidified material is different than that of the powder bed, thermal contours are created which consequently can cause part deformation due to the generated thermal stress [29,30]. Creation of keyhole porosity defects is also reported due to the simultaneous impact of high cooling rate and easy flow of molten material [31].

The purity of copper powder feedstock to the EB-PBF process is important as the amount of oxygen content present in the copper powder can be considerably detrimental to the properties of fabricated parts [32]. Even if the initial powder has low oxygen impurity, it has been found that reusing the copper powder in the EB-PBF for several cycles increases the oxygen content through creation of oxides in powder particles [33]. Thus, to produce high quality copper parts, the amount of oxygen content should be reduced and kept at low levels. Some oxygen reduction methods have been reported in the literature [34]. Hydrogen-treatment is one of the oxygen-reduction techniques and creates water molecules after exposing the oxidized copper powder particles to the flowing hydrogen gas. By heating the hydrogen-treated powder particles, the water molecules evaporate, and the oxygen content decreases [35,36]. Oxygen-reduction, which consequently results in less creation of oxides, has also been observed as a minor effect in the powders processed using another technique called the plasma spheroidization process, whose main objective is to improve the powder characteristics through reshaping the particles to spherical geometries [37–41]. As stated by Sehhat et al. in their comprehensive review paper on the plasma spheroidization process, the spheroidized powder has been found to have higher spherical particles, higher flowability, and lower oxygen impurity [42–44].

The powder feedstock needs to have sufficient flowability in order to ensure that the powder adequately spreads along the build plate during the EB-PBF process. The more spherical particle geometries result in better flowability and powder packing which consequently increases the powder bed density and improves the properties of fabricated parts [45–48]. Therefore, the powder feedstock to the EB-PBF process is recommended to be provided in spherical geometries. The plasma spheroidization process can be used to create such a powder feedstock by injecting the particles into a high-temperature plasma and reshaping them to spheres due to the created surface tension effects. Not only can the plasma spheroidization process reshape the particle geometries to spheres, but also it can reduce the oxygen impurities [49].

In this study, the impact of plasma spheroidization process on the morphology properties of copper powder, in terms of powder sphericity and particle size distribution, was investigated. The virgin powder was considered as the control case and its characteristics before and after the spheroidization were studied. To assess the impact of powder reuse on powder characteristics, the powder that was reused for 20 cycles in EB-PBF was characterized; then, to evaluate the capability of plasma spheroidization process in resetting the powder properties of used powder to its virgin-like conditions, the used powder was spheroidized and its properties were compared. In addition, to compare the oxygen-reduction capability of hydrogen-treatment process with that of plasma spheroidization process, a hydrogen-treated powder was spheroidized and the powders' oxygen content were measured. The effect of plasma spheroidization process on the powder's oxygen content was compared among all types of powders.

2. Material and methods

Three types of copper powder were characterized. The first type of powder is the gas-atomized copper powder in the as-received condition as purchased from the powder manufacturer and is called the virgin powder, which met UNS C10200 for oxygen-free high thermal conductivity (OFHC) copper (99.95 % purity and < 10 PPM oxygen content). After using the virgin powder in EB-PBF process for part fabrication, the unbuilt remaining powder can be collected to be reused as the input material feedstock for the next EB-PBF builds. The collected remaining powder after 20 times of recycling is called used powder and considered as the second type of characterized powder. The third type of powder is the same used powder as in the second type, but the powder underwent an oxygen-reduction treatment to reduce the oxygen content that the powder picked-up during EB-PBF process; the oxygen-reduced powder is called the reconditioned powder. The deployed oxygen-reduction technique was the hydrogen-treatment which was performed at 482 °C in a hydrogen atmosphere to reduce the surface oxides present on the samples. The furnace used for hydrogen-treatment was operating with flowing forming gas (Ar-5vol.%H2) at a rate of 120 cm^3/min. Table 1 summarizes the three types of powder characterized in this study and assigns a sample ID to each of them for easier reference in later discussions. Fig. 1 shows the three types of studied powders. The amount of oxygen present in a sample dominates the powder color as the used powder shows darker colors while the reconditioned powder reset to the initial bright color of virgin powder. To assess the flowability of three types of powder, the Revolution Powder Analyzer (RPA), which is composed of a digital camera taking images of powder motion in a rotating drum, was used. The results of powder avalanche angle (the maximum angle a powder creates in an avalanche) are shown in Table 2. A more flowable powder shows a smaller avalanche angle. Virgin powder was the most flowable powder, although its avalanche angle was slightly smaller than the reconditioned powder. The used powder had the least flowability, mainly due to the detrimental effects during powder recycling in AM. It should be noted that since the amount of powder collected after the spheroidization process was very small, it was not possible to measure the powder flowability of spheroidized powders.

For powder spheroidization, an Inductively Coupled Plasma (ICP) System, TekSphero-15, was used. The maximum power of this machine is 15 kW, and it is capable of providing plasma with temperatures as high as 3,000–10,000 K, which is high enough to decompose, melt, or evaporate most materials. An ASPEX Scanning Electron Microscope (SEM) was utilized to capture the SEM images

Table 1
Summary of characterized powders and their assigned sample ID.

Sample ID	Description
Virgin	As-purchased from the manufacturer
Used	As-purchased that was used for 20 build cycles in EB-PBF process
Reconditioned	Used for 20 build cycles in EB-PBF process and then oxygen-reduced

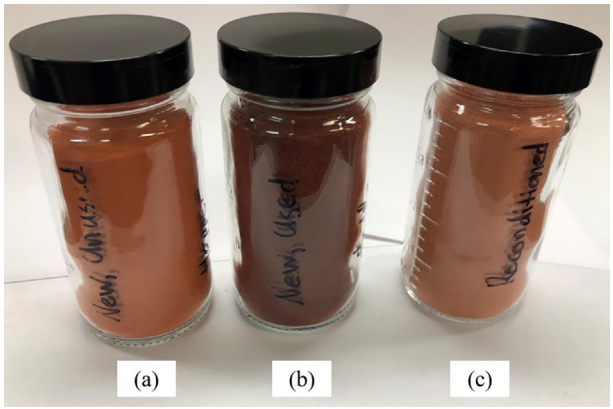

Fig. 1. The color of three types of powder, (a) virgin, (b) used in EB-PBF, (c) reconditioned (oxygen-reduced).

Table 2
Comparison of powder flowability in terms of avalanche angle (°).

Sample ID	Avalanche Angle
Virgin	29.6
Used	33.6
Reconditioned	30.8

of powder particles for morphology assessment. The powder particle sizes were measured using a particle size analyzer (Microtrac S3500) that works based on the laser diffraction method. The oxygen content was determined via LECO combustion analysis using a LECO ON836 analysis systems.

3. Experimental procedure

3.1. Spheroidization process

TekSphero-15 is an ICP machine that spheroidizes input powder, thereby improving the powder's flow characteristics while simultaneously removing unwanted impurities and reducing internal particle porosity. In addition to improving powder properties, a central goal of reconditioning powder is to reduce variations in powder properties and thus ultimately reduce uncertainty in the mechanical performance of manufactured parts. In the plasma spheroidization process the powder is injected into a high-temperature plasma under an inert atmosphere (cryogenic argon), to be melted for enhancing particle sphericity. The temperature of plasma is in the range of 3,000–10,000 K. Depending on the particle size, material melting point, residence time of powder particles in plasma, and spheroidization process parameters, the powder particles could be melted and/or vaporized. After powder particles are melted, they fall under gravity inside the plasma chamber, where they are quenched at the high cooling rates of $\sim 10^6$ K/s [50]. The surface tensions will alter the powder particle geometries to spheres.

The plasma-treated powder can be collected from two powder collection bins, including main bin and cyclone bin. The larger size powder is deposited in the main bin and the finer size powder is entrained to the cyclone bin. Depending on the needed particle size for the specific applications, different powder size from machine's different bins can be collected. Following the function of each spheroidization process parameter and considering the properties of copper powder, the levels for spheroidization process parameters should be appropriately selected to both reshape particles to spheres as best as possible and yield powder mass as highest as possible. Based on the findings of previous spheoidization studies and as recommended by the machine's manufacturer, the experiments were performed with carrier gas 3 lpm, central gas 10 lpm, and chamber pressure 15 psi. The used sheath gas was a mixture of Ar-H_2 (50 lpm cryogenic argon plus 4 lpm H_2) since addition of H_2 to argon had been found beneficial in protecting the torch against plasma high-temperatures and enlarging the plasma hot zone along the torch's axial direction [51,52].

3.2. Measurement of powder sphericity

After running the experiments, the powders were collected from both main and cyclone bins. Then, the particles were deposited on a carbon tape to prepare SEM samples. Ten SEM images per each sample were then taken to analyze the particle shapes, collecting data of at least 500 particles per sample. The SEM images were analyzed in MIPAR image analysis software. The change in powder shape was quantified using the aspect ratio, which is defined as the ratio of the major axis to the minor axis of the bounding ellipse for a particle. Through this definition, the particle sphericity increases as the aspect ratio approaches unity. The aspect ratio is reported in terms of cumulative percentage of powder particles; for example, AR_{50} = x indicates that the 50 % of particles of powder sample have aspect ratios smaller than or equal to x.

4. Results and discussion

4.1. Powder sphericity

The impact of powder type on sphericity of particles are individually compared. For each factor, first the comparison plots of powders collected from the main bin are discussed, followed by the same discussion for powders from the cyclone bin. To always have a comparison basis between as-received (shown as AR in the plots) powder and the powder spheroidized with different process parameters, the as-received powder's curve is included in all plots.

4.1.1. As-received of all powders

Before comparing the spheroidized powders, first the powder characteristics in their pre-spheroidization conditions (as-received) should be characterized. Fig. 2 shows the analysis of sphericity for the as-received conditions of all three types of powder. The used powder in the EB-PBF process shows almost the same sphericity as the virgin powder. Such finding can be desirable since from a particle geometry viewpoint, the particles were not deteriorated even after 20 times of recycling with the EB-PBF process. Based on this result, the powder can be reused for the next EB-PBF builds without concerning about particle sphericity. For the reconditioned powder (the oxygen-reduced used powder), the sphericity got worse, suggesting that during oxygen reconditioning treatment some detrimental effects were occurred to the particles' sphericity.

4.1.2. Virgin powder

Fig. 3 illustrates the particle geometries of virgin powder before and after spheroidization. The virgin powder is perfectly spheroidized in the main chamber while the spheroidized virgin powder collected from the cyclone bin shows irregular geometries. The sphericity of virgin powder in its as-received and spheroidized conditions can be seen in Fig. 4. The sphericity of powder collected from the main bin after spheroidization is shown in Fig. 4a, and that of the powder collected from the cyclone bin is displayed in Fig. 4b. The powder particles collected from the main bin show considerably higher sphericity after the spheroidization process

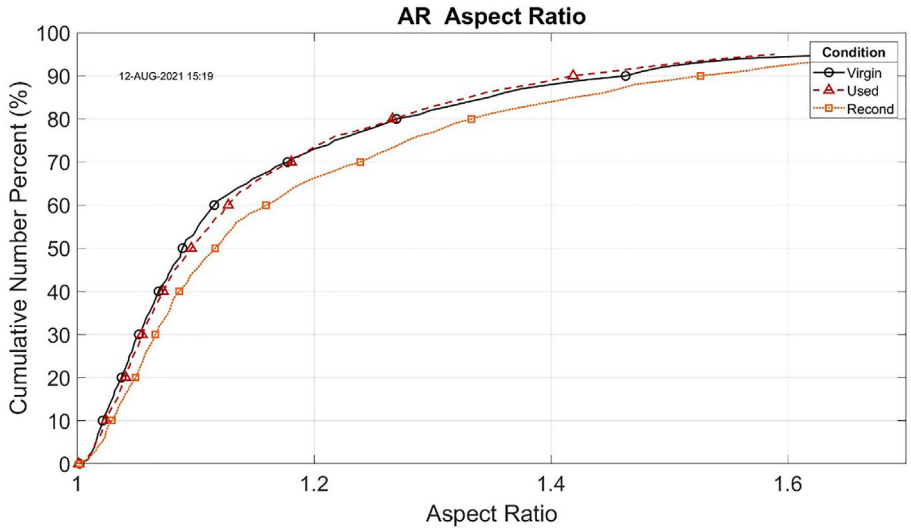

Fig. 2. Sphericity comparison of all three types of copper powders in their as-received conditions.

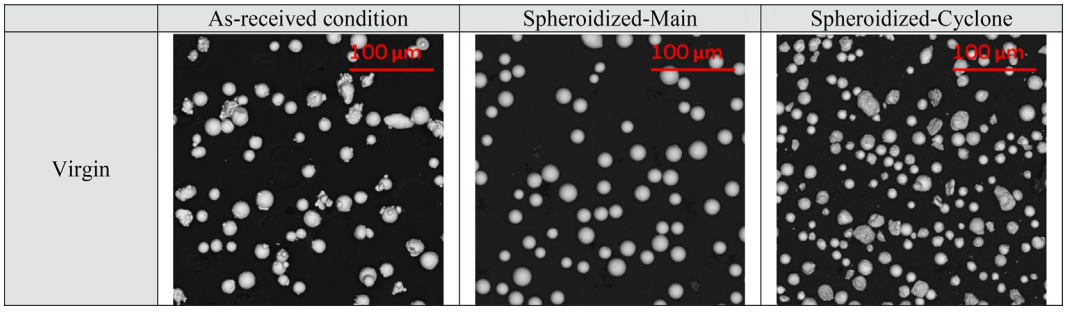

Fig. 3. SEM micrographs of virgin powder. Main bin powder shows higher sphericity while the cyclone bin powder shows similar sphericity to that of as-received powder. For powder in cyclone bin, the smaller molten droplets adhered to each other and created non-spherical particles.

while the powders in the cyclone bin show similar sphericity to that of their as-received condition. The sphericity deterioration of cyclone's powder can be explained by the smaller particle size for powder in cyclone bin; the smaller molten droplets adhered to each other and created non-spherical particles. Having said that, it should be noted that even the least spherical powder in this comparison, i.e., the virgin as-received powder particles, is still very spherical with aspect ratio values close to unity. For quantifying the powder yield, the mass of input powder and mass of powders collected from main and cyclone bins were measured and are reported in Table 3. As can be seen, one of the major system's downsides is the huge amount of powder residue on the machine's chamber wall, which requires manual removal and cleaning, and therefore is not usable.

4.1.3. Used powder

The SEM images corresponding to each powder condition are shown in Fig. 5. Appearance of several largely welded particles in the used1-main powder is observable; it seems several particles were adhered together during the melting step of spheroidization process and have created some large particles with satellites. In contrast, the used1-cyclone particles show high sphericity with small particle size; the appearance of satellites is rare in the used1-cyclone. As mentioned, it should be noted that the used1-main powder was fed as the as-received condition of the second round of spheroidization. The used2-main powder is composed of large particles with sharp edges; the solidification striation lines are left on particle surfaces at the intersection areas of welded multi-particles which are caused by the impact of second round of particle re-heating and surface tension re-creation. The same is true for used2-cyclone with smaller sizes.

The sphericity of used powder in three conditions of as-received, after first round of spheroidization (called spheroidized-used), and after second round of spheroidization (called spheroidized-used2) are shown in Fig. 6. First the used as-received powder was fed into the machine and the spheroidized-used powder was collected from both the main and cyclone bins. Then, the spheroidized-used powder collected from the main bin was fed into the machine for the second round of spheroidization. For the used powder, the sphericity of particles showed minimal improvement by re-spheroidizing the powder collected from the main bin; the order of powder sphericity from highest to lowest for used powder from the main bins is spheroidized-used2 > spheroidized-used > as-received, as shown in Fig. 6a. It should be noted that the plots display the *cumulative* distribution of aspect ratio. During powder spheroidization the smaller particles evaporate due to the plasma high temperatures. By removing these small-size particles which are usually in irregular geometries, the remained powder is only composed of large-size particles which are usually spherical. When considering the particles' aspect ratio in a *cumulative* manner, the removal of small-size particles plays an important role. Thus, the increase in sphericity of particles after re-spheroidization shown in Fig. 6a is mainly due to the removal of small-size particles and not necessarily reshaping the particles. For the powders collected from the cyclone, the first round of spheroidization minimally improved the particles'

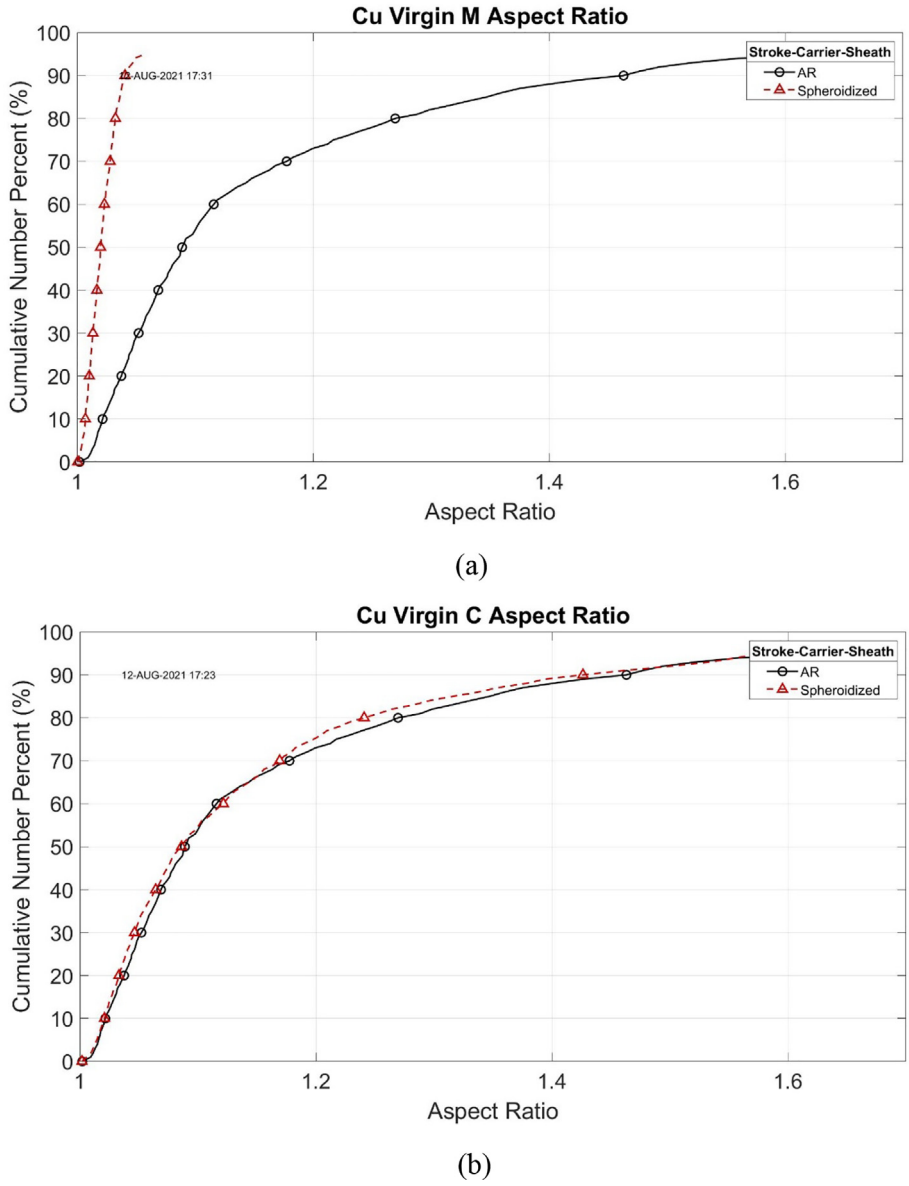

Fig. 4. The sphericity of virgin powder particles in their as-received and spheroidized conditions for powders collected from, (a) the main bin, and (b) the cyclone bin.

Table 3
The quantity of input powder and yield (g).

Input Mass	Main Bin	Cyclone Bin	Chamber Wall's Residual
50.63	13.73	0.72	23.68

sphericity due to the evaporation of small-size particles with irregular geometries, as shown in Fig. 6b. Although the second round of spheroidization caused partially better sphericity than the as-received condition, the second round of spheroidization resulted in less sphericity than the first round of spheroidization. This can be explained by two facts. Firstly, it should be noted that the input powder for the second round of spheroidization was the used1-main. Secondly, the used2-c has fewer small-size particles than used1-m (the fed powder for the second round of spheroidization), thus, the first cumulative percentiles of the used2-c powder (until 70 percentile) shows higher sphericity than that of the as-received condition; however, after 70 percentile, the used2-c powder shows worse sphericity since after two cycles of evaporation, the used2-c powder has lost several particles and is left with only large particles with geometries less spherical than that of the as-received condition.

4.1.4. Reconditioned powder

The SEM images of reconditioned powder before and after spheroidization are shown in Fig. 7. Reconditioned-main powder shows high sphericity while the sphericity of reconditioned-cyclone powder is perfect. The sphericity of reconditioned powder is compared in Fig. 8 for powders collected from both main and cyclone bins. The reconditioned powders showed higher sphericity after the plasma spheroidization in both main and cyclone bins.

4.1.5. Spheroidized of all powders

To make a deeper comparison and discussion among the three types of powder, Fig. 9 shows the spheroidized condi-

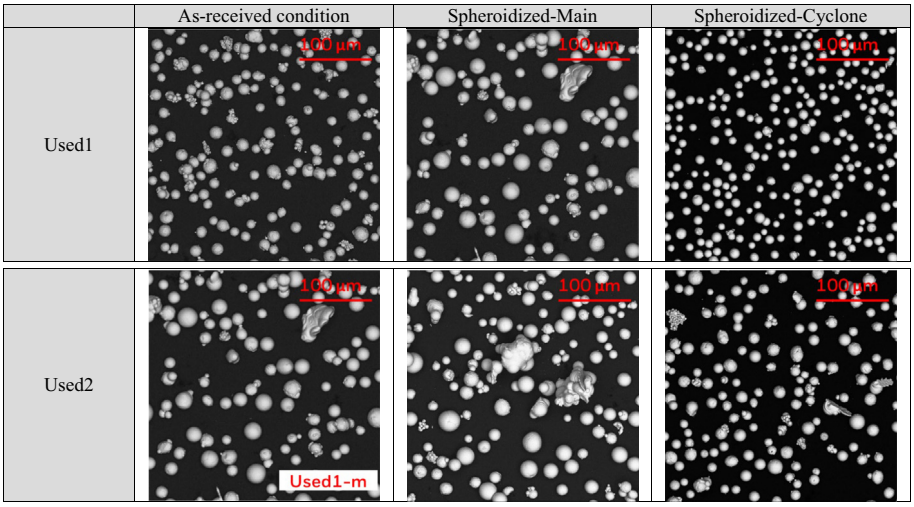

Fig. 5. SEM micrographs of used powder. Top and bottom rows show the powder conditions for the first and second round of spheoidization, respectively. re-spheroidization improved the sphericity of main bin powder while it deteriorated the sphericity of cyclone bin powder.

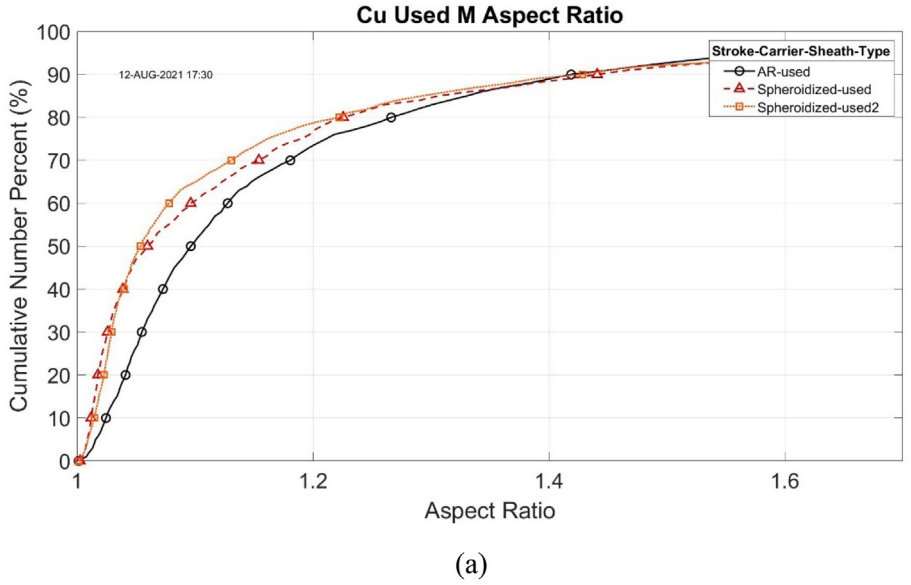

Fig. 6. The sphericity of used powder particles in their as-received, first spheroidization round, and second spheoidization round for powders collected from, (a) the main bin, and (b) the cyclone bin.

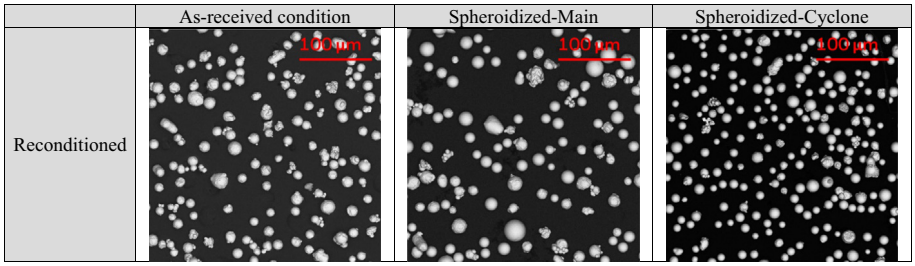

Fig. 7. SEM micrographs of reconditioned powder. Both main bin and cyclone bin powders showed improved sphericity compared to their as-received conditions.

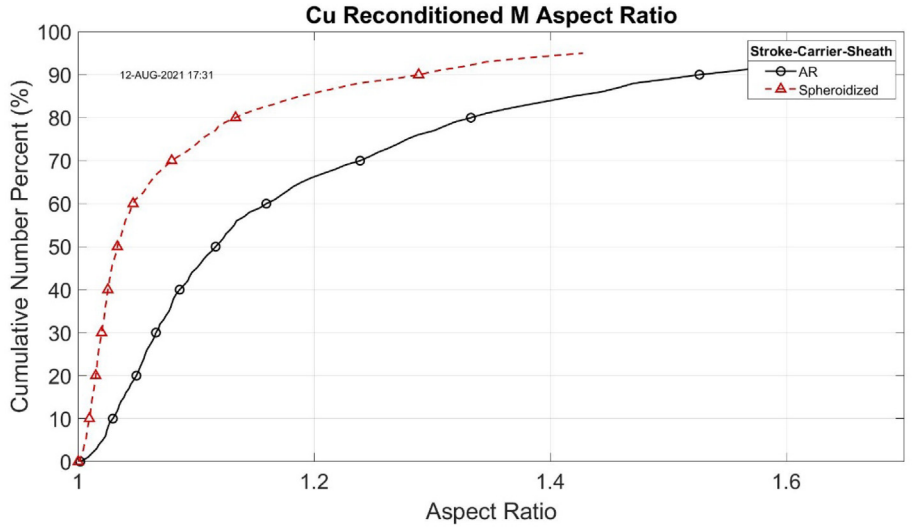

(a)

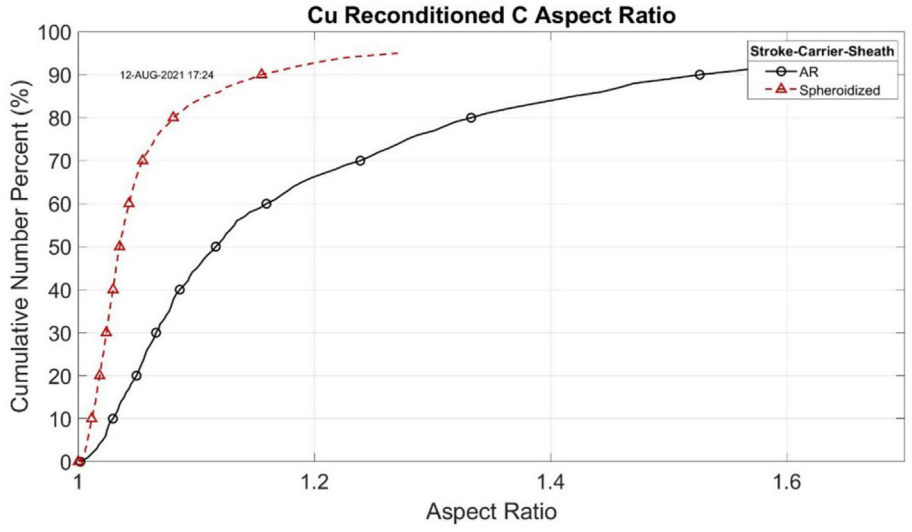

(b)

Fig. 8. The sphericity of reconditioned powder particles in their as-received, spheroidized conditions for powders collected from, (a) the main bin, and (b) the cyclone bin.

tions of all powders in both main and cyclone bins. The baseline material, i.e., virgin powder in its as-received condition (AR-virgin) is also included in the plots to facilitate making an inclusive comparison. For powders collected from the main bin, the spheroidized-virgin powder resulted in the highest spherical particles. The first round of spheroidization on the used powder made the particles more spherical compared to the AR-virgin; in other words, the spheroidized-used powder showed higher sphericity than the AR-virgin. The second round of spheoidization (spheroidized-used2) improved powder sphericity compared to as-received-virgin while it shows comparable sphericity to that of spheroidized-used1. The spheroidized-reconditioned powder shows improvement in its sphericity. These changes in pow-

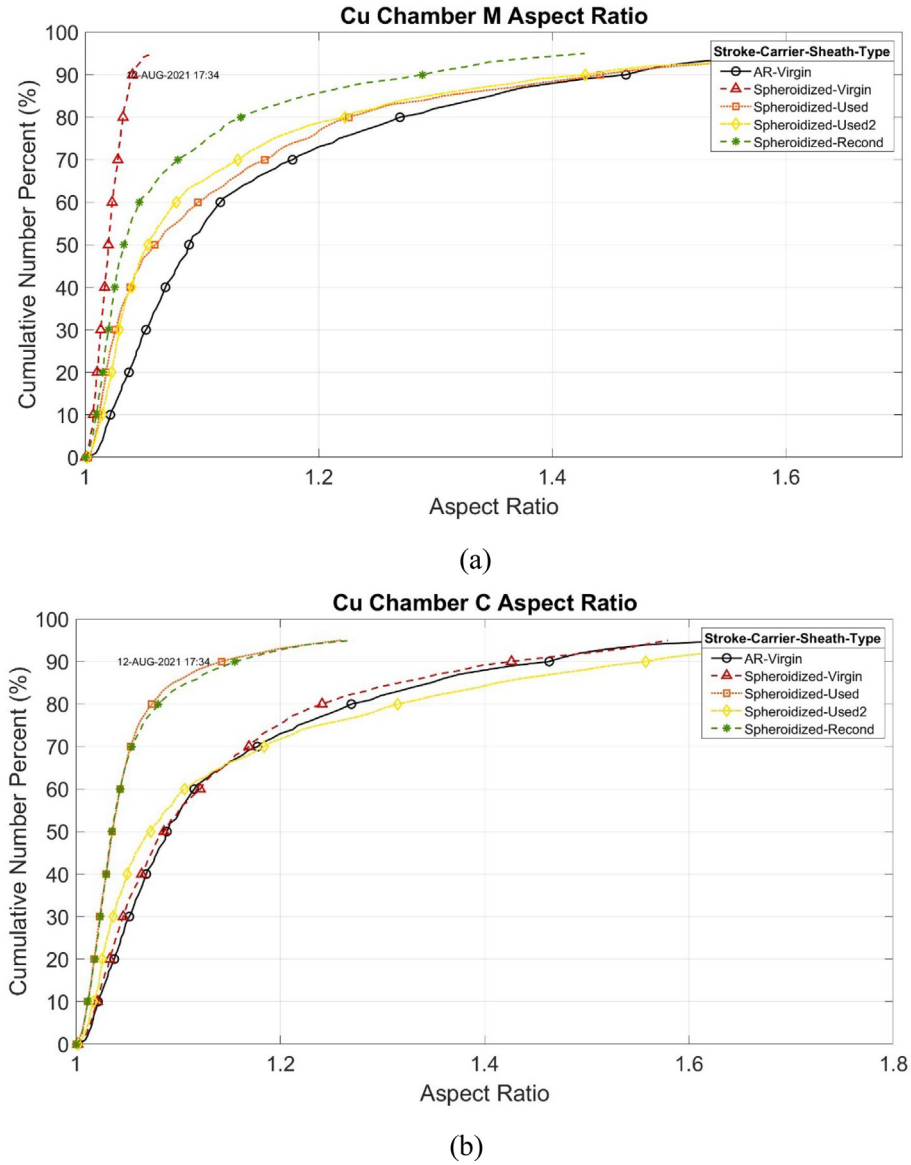

Fig. 9. Comparison among the spheroidized conditions of different types of powder for powders collected from, (a) the main bin, and (b) the cyclone bin.

der sphericity can be correlated with the change in powders' oxygen content, as discussed in the next sections.

For the powders collected from the cyclone bin (see Fig. 9b), the spheroidized-virgin powder showed slightly higher sphericity than the AR-virgin powder. The first round of spheroidization on the used powder improved the powder sphericity considerably while the second round of spheroidization deteriorated the powder sphericity to the same level of AR-virgin powder. The sphericity of reconditioned powder was improved to the similar sphericity of spheroidized-used1 powder, indicating that the hydrogen-treatment had no impact on the sphericity of particles collected from the cyclone bin. In other word, although the reconditioned powder had less oxygen content than the used powder, they both showed same sphericity after the spheroidization process.

4.2. Particle size distribution

As highlighted in the previous sections, one of the important factors in the powder spheroidization process is the powder evaporation which changes particle size distributions through vaporizing the fine particles. Thus, besides the particle sphericity, the particle size distribution should be studied. Following the same discussion layout for the powder sphericity, in the below sections first the particle size distribution of powders in their as-received conditions are compared followed by an individual discussion on each type of powder.

4.2.1. As-received of all powders

The comparison for all types of powder in their as-received conditions are shown in Fig. 10. The virgin powder has more small-size particles than that of the used and reconditioned powders. As the reconditioned powder is the same used powder but with less oxygen, the used and reconditioned powders have similar particle size and are larger than the virgin powder; this is confirmed by a shift in particle size peak to larger values.

4.2.2. Virgin powder

Fig. 11 shows the particle size distribution for virgin as-received powders collected from the main and cyclone bins. For the main chamber, not only the spheroidized powder has fewer small-size

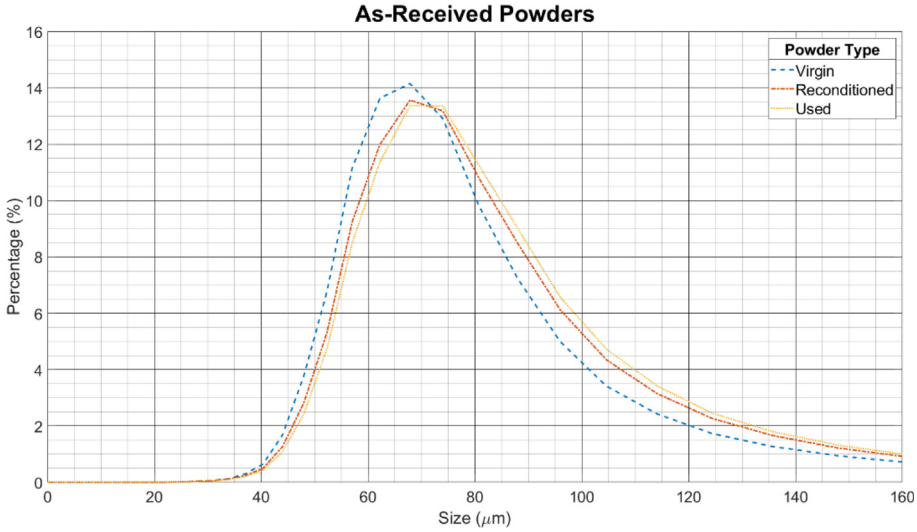

Fig. 10. Particle size distribution comparison of all three types of copper powders in their as-received conditions.

particles, but also several particles are enlarged to greater sizes (Fig. 11a). This could be due to both evaporation and particle reshaping to spheres during the spheroidization process. For the cyclone bin, the particle size decreased considerably as can be seen in Fig. 11b. The spheroidization machine operates in way that smaller size particles will be entrained and collected in the cyclone bin.

4.2.3. Used powder

The comparison for the used powder from the main and cyclone bins in three conditions of as-received, after the first round of spheroidization (called spheroidized-1), and after second round of spheroidization (called spheroidized-2) is shown in Fig. 12. For the powders collected from the main bins, the spheroidized-1 powder has fewer small-size particles and a greater number of large-size particles. This suggests that the finer particles were evaporated and some of the large particles were melted and agglomerated with other particles to create even larger size particles during the spheroidization process. Second round of spheroidization increased the number of finer particles although it should have been reduced due to the second evaporation round of finer size particles. For the powders collected from the cyclone bin, the particle size of spheroidized-1 decreased while the particle size of spheroidized-2 increased; this can be caused by feeding spheroidized-1-main as input for the second round of spheroidization, confirmed by the similarity in particle size distribution of spheroidized-1 with spheroidized-2-cyclone as can be compared by looking at Fig. 12a and Fig. 12b.

4.2.4. Reconditioned powder

The impact of spheroidization process on powder particle size distribution of oxygen-reduced powder for both main and cyclone bins is shown in Fig. 13. For powders collected from the main bin, spheroidized powder shows fewer small-size particles and the particles are reshaped to larger ones. For the powders collected from the cyclone bin, the particles reshape to smaller sizes, as shown in Fig. 13b.

4.2.5. Spheroidized of all powders

For a comparison among all the spheroidized powders in terms of their particle size distributions, powders collected from both main and cyclone bins of all spheroidized powders were compared as shown in Fig. 14. The virgin as-received powder is also included in all plots as a comparison baseline. For the powders collected from the main chamber, the virgin spheroidized powder shows fewer small-size particles compared with the virgin as-received powder. The same is true for the used1, used2, and reconditioned powders. The used2 powder shows a greater number of smaller particles than that of the used1. The reconditioned powder, however, shows even smaller sizes than those of both used1 and used2. For the powders collected from the cyclone (see Fig. 14b), the spheroidized virgin is composed of more small-size particles than any other powder type. The first round of spheroidization has several small-size particles while the second round of spheroidization shifted particle size to greater values. The reconditioned powder has fewer small-size particles than that of the used1 powder.

5. Oxygen impurity and created grooves

As mentioned earlier, the treatment method for reconditioned powder was to expose the used powder to flowing forming gas which reacts with the present oxides in the powder to create H_2O molecules. By heating the hydrogen-treated powder to high temperatures (beyond 400 °C), the created H_2O molecules evaporate as water vapor. Ledford et al. [36] found that when the water vapor is leaving the powder particles, it leaves some grooves both on the particles surfaces and among the individual particles' grain boundaries. These grooves were found to remain on the particles surfaces even when the powder is set back to the room environment conditions. To evaluate the creation of such grooves in different types of powders after the plasma spheroidization process and whether the water evaporation is the main cause of groove creation, the oxygen content of powders collected from the main bin was measured and compared corresponding to the observed grooves in their SEM micrographs.

Table 4 shows the measured values of oxygen content in different types of powder before and after the spheroidization process. The oxygen content in the virgin powder decreased from 200 to 40 ppm after the spheroidization since the plasma spheroidization process provides high enough temperatures to remove oxygen from powder particles. The powder used for 20 cycles in the EB-PBF process considerably picked up oxygen from 200 ppm (virgin-as-received condition) to high value of 370 ppm; one round of spheroidization on this used powder decreased the oxygen impurity to 120 ppm. Not only is the oxygen content present in

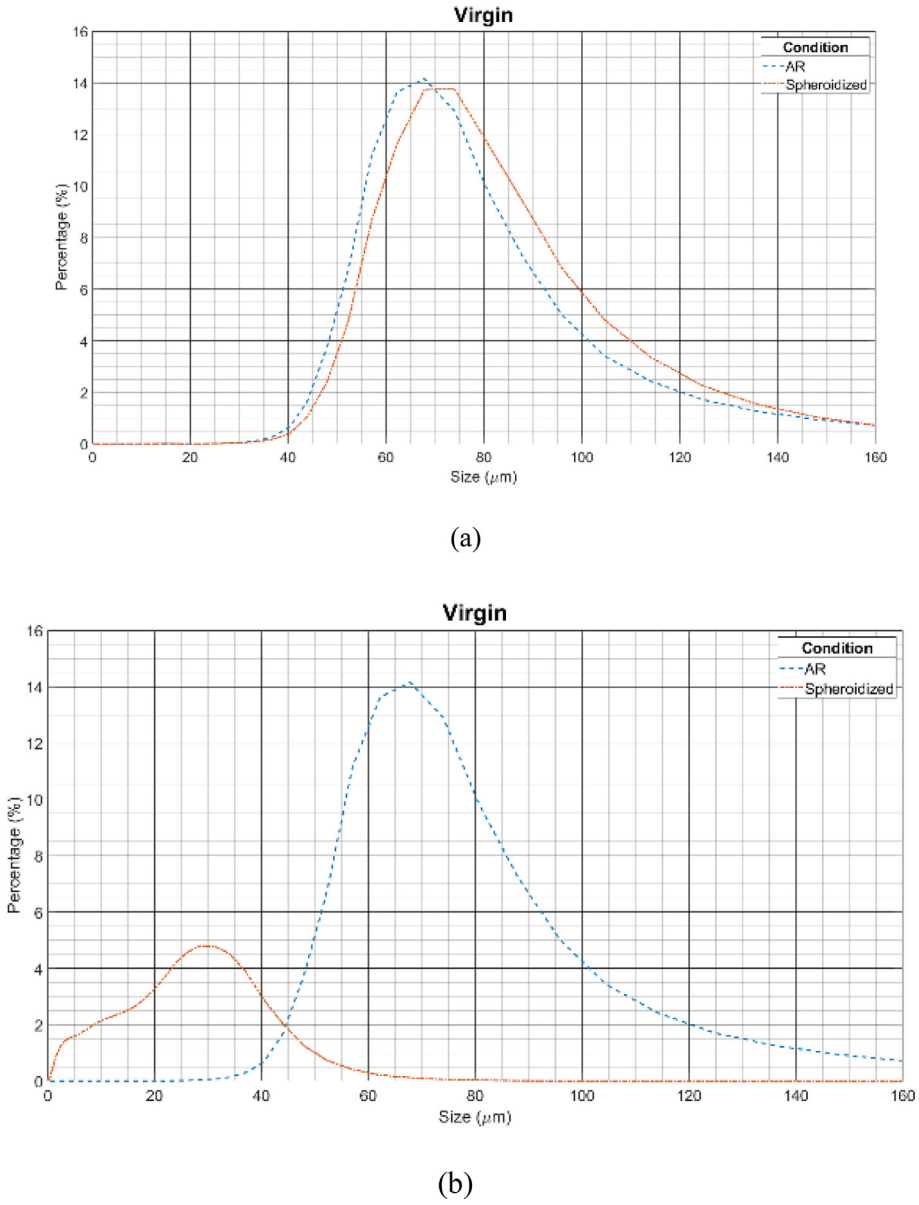

Fig. 11. The particle size distribution of virgin powder particles in their as-received and spheroidized conditions for powders collected from the main bin (a), and the cyclone bin (b).

the used-spheroidized powder much less than that of its pre-spheroidization condition (120 vs 370 ppm), but also the used-spheroidized powder has lower oxygen content than that of the virgin-as-received powder (120 vs 200 ppm). These are promising signs as they indicate the oxygen-reducing capability of spheroidization process to decrease the oxygen content to values even lower than that of the as-received powder. In contrast to one's intuition that re-spheroidization may be even more beneficial in decreasing the powder's oxygen impurity, the second round of spheroidization showed no variation in oxygen content (constant at 120 ppm); based on the collected data in this study, re-spheroidizing the powder for the second round of spheroidization caused no change in the powder's oxygen content. The further rounds of re-spheroidization, i.e., third round, fourth round, etc., may cause a change in powder's oxygen content, evaluation of which will be a future work of this study. The reconditioned powder had less oxygen content than the virgin (140 vs 200 ppm) and used (140 vs 370 ppm) powders before their spheroidization which implicates the functionality of hydrogen-treatment process in reducing the powder's oxygen content. Spheroidizing the reconditioned powder decreased its oxygen content from 140 to 80 ppm; although the oxygen present in the reconditioned-spheroidized powder is less than that of the used-spheroidized powder (80 vs 120 ppm), the spheroidized-virgin powder still showed the least oxygen impurity (40 ppm) among all powders. This finding suggests that the direct spheroidization process without a pre-hydrogen-treatment is more powerful in decreasing the powder's oxygen content and outperforms both the hydrogen-treatment process and the spheroidization process with a pre-hydrogen-treatment in this regard. While not a major contributor, we believe that using a mixture of Ar-H_2 as the sheath gas helps to keep the oxygen partial pressure low, which is probably the main reason for the deoxidation of the powder. Thus, if the powder is planned to be processed with the plasma spheoidization, there is no need

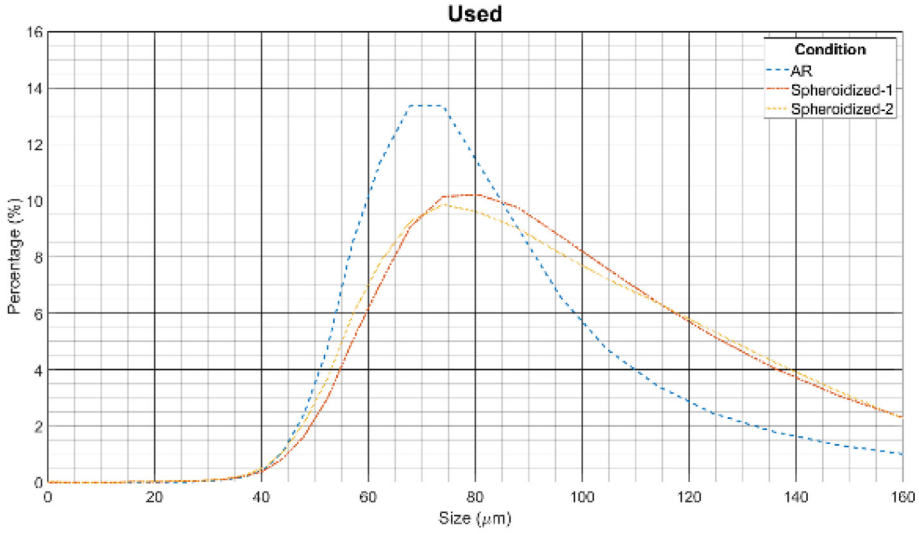

(a)

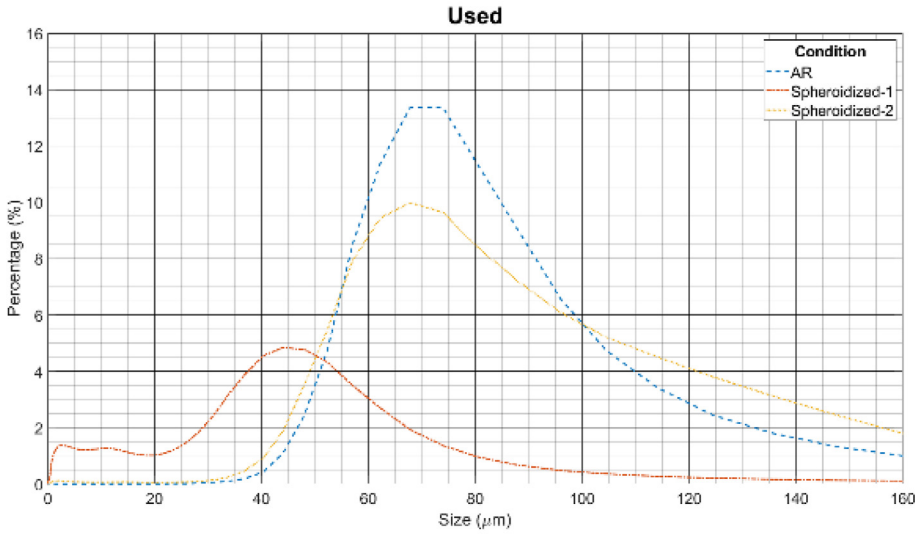

(b)

Fig. 12. The particle size distribution of used powder particles in their as-received and spheroidized conditions for powders collected from the main bin (a), and the cyclone bin (b).

of powder hydrogen-treatment prior to the spheroidization process.

A correlation between the oxygen content and the powder sphericity was observed. The spheroidized-virgin powder had very low oxygen content among all spheroidized powders. The lower oxygen impurity in a powder is mainly due to the existence of less oxides on the particle surfaces. The spheroidized-virgin powder particles collected from the main bin showed considerably higher sphericity after the spheroidization process since a smaller number of oxides existed on the particle surfaces after the spheroidization process. The same pattern was observed for the reconditioned powder where the consistent sphericity improvement in both main and cyclone bins of reconditioned powder is because the reconditioned powder particles have less surface oxides.

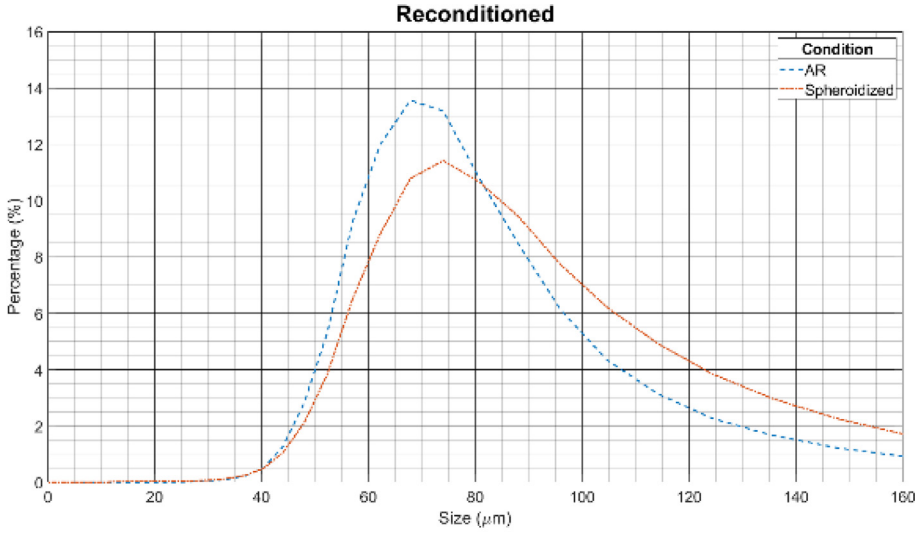

(a)

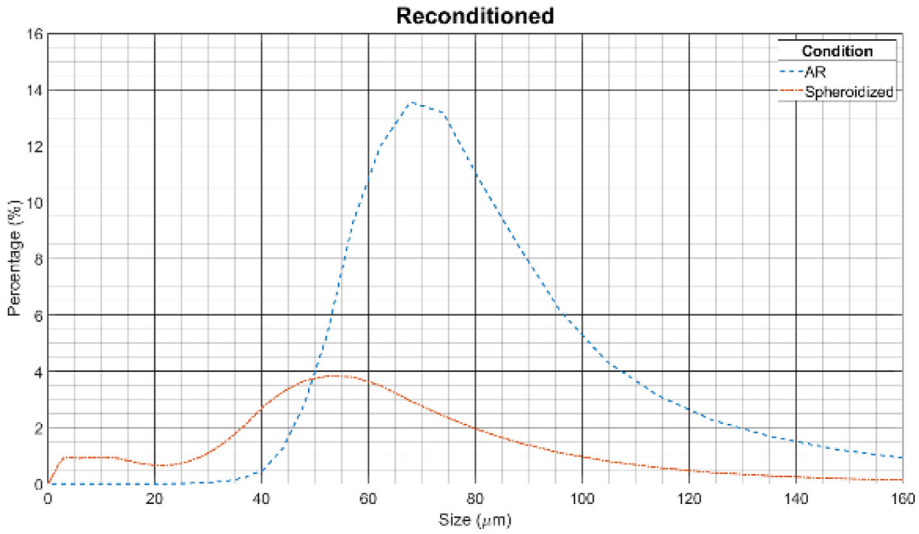

(b)

Fig. 13. The particle size distribution of reconditioned powder particles in their as-received and spheroidized conditions for powders collected from the main bin (a), and the cyclone bin (b).

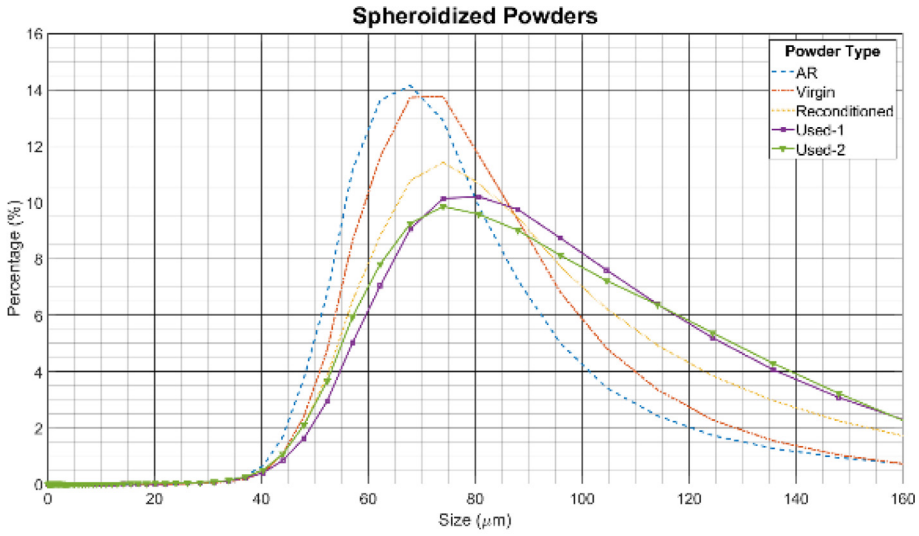

(a)

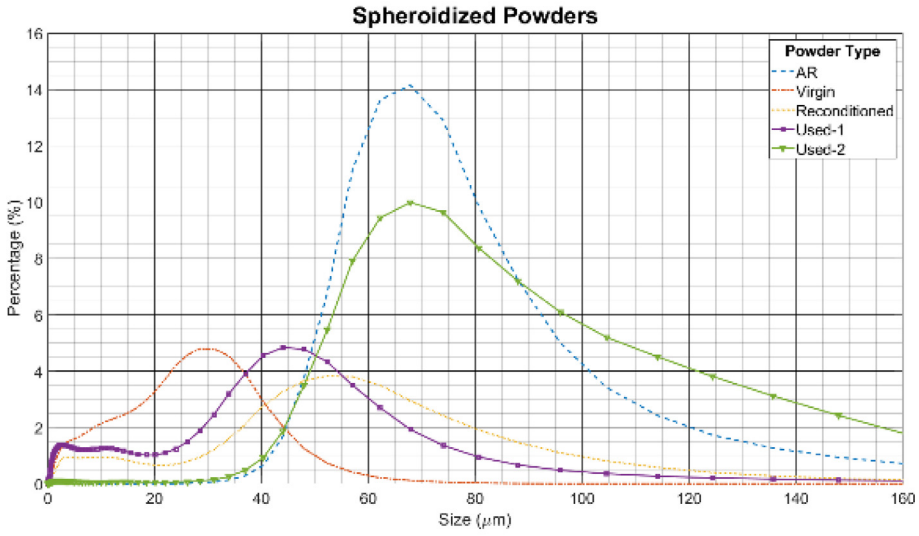

(b)

Fig. 14. Particle size distribution comparison among the spheroidized conditions of different types of powders collected from, (a) the main bin, and (b) the cyclone bin.

Table 4
The oxygen content in different types of powder before and after the spheoidization.

Powder	As-received (ppm)	Spheroidized (ppm)
Virgin	200	40
Used	370	120
Used-second spheroidization	120	120
Reconditioned	140	80

6. Conclusion

In this work, three types of copper powder, including virgin, used in EB-PBF process, and oxygen-reduced after being used in EB-PBF process, were plasma spheroidized using process parameters stroke 50 %, carrier gas 3 lpm, sheath gas 50 lpm. For the used powder the spheroidization was performed for the second round to evaluate the impact of re-spheroidization on powder properties. The spheroidization process reshaped the powder particles to more spherical geometries. The powders collected from machine's different bins were influenced differently after the second spheroidization round as the sphericity of main bin's powder improved while the sphericity of cyclone bin's powder deteriorated. Although, the powders collected from the main chamber show fewer small-size particles overall, the second spheroidization round created a greater number of smaller particles than that of the first spheroidization round. For the powders collected from the cyclone bin, the first round of spheroidization created several small-size particles while the second round of spheroidization shifted particle size to larger values. The spheroidization process was found to decrease the oxygen content of these studied copper powders. In addition to improving the geometry and uniforming the particle size distribution, the spheroidization of used powder reset the powder's oxygen content to values lower than that of the virgin-as-received powder. This indicates the advantageous impact of spheroidization process in powder re-use. The second round of spheroidization showed no variation in oxygen content. The spheroidization process also outperformed the hydrogen-

treatment method as the spheroidized-virgin powder showed lower oxygen impurity than that of the reconditioned powder.

Declaration of Competing Interest

The authors declare that they have no known competing financial interests or personal relationships that could have appeared to influence the work reported in this paper.

Acknowledgments

This work was funded by Honeywell Federal Manufacturing & Technologies LLC under Contract No. DE-NA0002839 with the U. S. Department of Energy. The United States Government retains and the publisher, by accepting the article for publication, acknowledges that the United States Government retains a nonexclusive, paid-up, irrevocable, worldwide license to publish or reproduce the published form of this manuscript, or allow others to do so, for the United States Government purposes.

References

[1] B. Behdani, M. Senter, L. Mason, M. Leu, J. Park, Numerical Study on the Temperature-Dependent Viscosity Effect on the Strand Shape in Extrusion-Based Additive Manufacturing, J. Manuf. Mater. Process. 4 (2020) 46, https://doi.org/10.3390/jmmp4020046.

[2] M.H. Sehhat, A. Mahdianikhotbesara, F. Yadegari, Impact of temperature and material variation on mechanical properties of parts fabricated with fused deposition modeling (FDM) additive manufacturing, Int. J. Adv. Manuf. Technol. 120 (7-8) (2022) 4791–4801, https://doi.org/10.1007/S00170-022-09043-0.

[3] M.H. Sehhat, A. Mahdianikhotbesara, F. Yadegari, Verification of stress transformation in anisotropic material additively manufactured by fused deposition modeling (FDM), Int. J. Adv. Manuf. Technol. 2022 (2022) 1–7, https://doi.org/10.1007/S00170-022-10321-0.

[4] M.H. Sehhat, A. Mahdianikhotbesara, M. Hadad, Formability Investigation for Perforated Steel Sheets, SAE Int. J. Mater. Manuf. 15 (2022), https://doi.org/10.4271/05-15-02-0012, 05–15-02–0012.

[5] A. Mahdianikhotbesara, M.H. Sehhat, M. Hadad, Experimental Study on Micro-Friction Stir Welding of Dissimilar Butt Joints Between Al 1050 and Pure Copper, Metallogr. Microstruct. Anal. 2021 (2021) 1–16, https://doi.org/10.1007/S13632-021-00771-5.

[6] C.H. Hung, W.T. Chen, M.H. Sehhat, M.C. Leu, The effect of laser welding modes on mechanical properties and microstructure of 304L stainless steel parts fabricated by laser-foil-printing additive manufacturing, Int. J. Adv. Manuf. Technol. (2020) 1–11, https://doi.org/10.1007/s00170-020-06402-7.

[7] V. Chenarani, A. Mahdianikhotbesara, M. Hadad, M.H. Sehhat, M. Hedayati-Dezfooli, A. Zaheri, A. Araee, Evaluation of the Forming Limit Diagram (FLD) for St-Mg-St Multilayer Sheet Manufactured by Transient Liquid Phase (TLP) Bonding, Metallogr. Microstruct. Anal. 2022 (2022) 1–13, https://doi.org/10.1007/S13632-022-00904-4.

[8] M. Hadad, J. Gholampour Darzi, A. Mahdianikhotbesara, J. Makarian, Experimental investigation of the effect of single point dressing parameters on grinding of Mo40 hardened steel using mounted point grinding tool, Energy Equip. Syst. 10 (2022) 197–214, https://doi.org/10.22059/EES.2022.253231.

[9] M.H. Sehhat, B. Behdani, C.-H. Hung, A. Mahdianikhotbesara, Development of an Empirical Model on Melt Pool Variation in Laser Foil Printing Additive Manufacturing Process Using Statistical Analysis, Metallogr. Microstruct. Anal. 2021 (2021) 1–8, https://doi.org/10.1007/S13632-021-00795-X.

[10] C.-H. Hung, T. Turk, M.H. Sehhat, M.C. Leu, Development and experimental study of an automated laser-foilprinting additive manufacturing system, Rapid Prototyp. J. 28 (6) (2022) 1013–1022, https://doi.org/10.1108/RPJ-10-2021-0269, ahead-of-print.

[11] T. Turk, C.-H. Hung, M. Hossein Sehhat, M.C. Leu, Methods of Automating the Laser-Foil-Printing Additive Manufacturing Process, in: 2021 Int. Solid Free. Fabr. Symp. University of Texas at Austin, 2021.

[12] A. Mahdianikhotbesara, M.H. Sehhat, M. Hadad, A Numerical and Experimental Study into Thermal Behavior of Micro Friction Stir Welded Joints of Al 1050 and Copper Sheets, Adv. Mater. Res. 1170 (2022) 49–60, https://doi.org/10.4028/P-01AG12.

[13] M.H. Sehhat, · Ali Mahdianikhotbesara, Powder spreading in laser-powder bed fusion process 23 (2021) 89, https://doi.org/10.1007/s10035-021-01162-x.

[14] X. Deng, Z. Huang, W. Wang, R.N. Davé, Investigation of nanoparticle agglomerates properties using Monte Carlo simulations, Adv. Powder Technol. 27 (2016) 1971–1979, https://doi.org/10.1016/J.APT.2016.06.029.

[15] Y. Chen, L. Jallo, M.A.S. Quintanilla, R. Dave, Characterization of particle and bulk level cohesion reduction of surface modified fine aluminum powders, Colloids Surfaces A Physicochem. Eng. Asp. 361 (2010) 66–80, https://doi.org/10.1016/J.COLSURFA.2010.03.015.

[16] Z. Huang, K.T. Kunnath, X. Han, X. Deng, L. Chen, R.N. Davé, Ultra-fine dispersible powders coated with l-Leucine via two-step co-milling, Adv. Powder Technol. 29 (2018) 2957–2965, https://doi.org/10.1016/J.APT.2018.10.015.

[17] J. Yang, Y. Wang, R.N. Dave, R. Pfeffer, Mixing of nano-particles by rapid expansion of high-pressure suspensions, Adv. Powder Technol. 14 (2003) 471–493, https://doi.org/10.1163/156855203769710681.

[18] M. Azad, G. Guner, A. Afolabi, R. Davé, E. Bilgili, Impact of solvents during wet stirred media milling of cross-linked biopolymer suspensions, Adv. Powder Technol. 32 (2021) 4562–4575, https://doi.org/10.1016/J.APT.2021.10.007.

[19] P.D. Nezhadfar, S. Thompson, A. Saharan, N. Phan, N. Shamsaei, Fatigue and Failure Analysis of an Additively Manufactured Contemporary Aluminum Alloy, in: Miner. Met. Mater. Ser., Springer Science and Business Media Deutschland GmbH, 2021: pp. 212–219. https://doi.org/10.1007/978-3-030-65396-5_31.

[20] A.P. Jirandehi, M.M. Khonsari, General quantification of fatigue damage with provision for microstructure: A review, Fatigue Fract, Eng. Mater. Struct. (2021) ffe.13515, https://doi.org/10.1111/ffe.13515.

[21] H. Ghadimi, A.P. Jirandehi, S. Nemati, S. Guo, Small-sized specimen design with the provision for high-frequency bending-fatigue testing, Fatigue Fract. Eng. Mater. Struct. (2021), https://doi.org/10.1111/FFE.13589.

[22] J. Yang, A. Sliva, A. Banerjee, R.N. Dave, R. Pfeffer, Dry particle coating for improving the flowability of cohesive powders, Powder Technol. 158 (2005) 21–33, https://doi.org/10.1016/J.POWTEC.2005.04.032.

[23] L.J. Jallo, M. Schoenitz, E.L. Dreizin, R.N. Dave, C.E. Johnson, The effect of surface modification of aluminum powder on its flowability, combustion and reactivity, Powder Technol. 204 (2010) 63–70, https://doi.org/10.1016/J.POWTEC.2010.07.017.

[24] R. Dave, W. Chen, A. Mujumdar, W. Wang, R. Pfeffer, Numerical simulation of dry particle coating processes by the discrete element method, Adv. Powder Technol. 14 (2003) 449–470, https://doi.org/10.1163/156855203769710672.

[25] G. Yang, P. Yang, K. Yang, N. Liu, L. Jia, J. Wang, H. Tang, Effect of processing parameters on the density, microstructure and strength of pure tungsten fabricated by selective electron beam melting, Int. J. Refract. Met. Hard Mater. 84 (2019), https://doi.org/10.1016/J.IJRMHM.2019.105040.

[26] M. Brochu, P. Wanjara, Transient liquid phase bonding of Cu to Cu–W composite using an electron beam energy source, Int. J. Refract. Met. Hard Mater. 25 (2007) 67–71, https://doi.org/10.1016/J.IJRMHM.2006.01.001.

[27] S.J. Raab, R. Guschlbauer, M.A. Lodes, C. Körner, Thermal and Electrical Conductivity of 99.9% Pure Copper Processed via Selective Electron Beam Melting, Adv. Eng. Mater. 18 (2016) 1661–1666, https://doi.org/10.1002/ADEM.201600078.

[28] R. Guschlbauer, S. Momeni, F. Osmanlic, C. Körner, Process development of 99.95% pure copper processed via selective electron beam melting and its mechanical and physical properties, Mater. Charact. 143 (2018) 163–170, https://doi.org/10.1016/J.MATCHAR.2018.04.009.

[29] C.J. Smith, S. Tammas-Williams, E. Hernandez-Nava, I. Todd, Tailoring the thermal conductivity of the powder bed in Electron Beam Melting (EBM) Additive Manufacturing, Sci. Reports 2017 71. 7 (2017) 1–8. https://doi.org/10.1038/s41598-017-11243-8.

[30] L.C. Wei, L.E. Ehrlich, M.J. Powell-Palm, C. Montgomery, J. Beuth, J.A. Malen, Thermal conductivity of metal powders for powder bed additive manufacturing, Addit. Manuf. 21 (2018) 201–208, https://doi.org/10.1016/J.ADDMA.2018.02.002.

[31] A.A. Martin, N.P. Calta, J.A. Hammons, S.A. Khairallah, M.H. Nielsen, R.M. Shuttlesworth, N. Sinclair, M.J. Matthews, J.R. Jeffries, T.M. Willey, J.R.I. Lee, Ultrafast dynamics of laser-metal interactions in additive manufacturing alloys captured by in situ X-ray imaging, Mater. Today Adv. 1 (2019), https://doi.org/10.1016/J.MTADV.2019.01.001.

[32] E. Belkin, P.K. Nagata, Hydrogen Embrittlement of Tough Pitch Copper by Brazing Testing the effects of six variables statistically shows factors that can cause, enhance, or have no effect on embrittlement, (n.d.).

[33] P. Frigola, O.A. Harrysson, T.J. Horn, H.A. West, R.L. Aman, J.M. Rigsbee, D.A. Ramirez, L.E. Murr, F. Medina, R.B. Wicker, E. Rodriguez, Fabricating Copper Components with Electron Beam Melting, (2014). www.arcam.com/CommonResources/Files/www.arcam.com/ (accessed October 6, 2021).

[34] Y. Zhang, W. Lu, P. Sun, Z.Z. Fang, S. Qiao, Y. Zhang, S. Zheng, Deoxygenation of Ti metal: A review of processes in literature, Int. J. Refract. Met. Hard Mater. 91 (2020), https://doi.org/10.1016/J.IJRMHM.2020.105270.

[35] T.I. El-Wardany, Y. She, V.N. Jagdale, J.K. Garofano, J.J. Liou, W.R. Schmidt, Challenges in Three-Dimensional Printing of High-Conductivity Copper, J. Electron. Packag. 140 (2018), https://doi.org/10.1115/1.4039974.

[36] C. Ledford, C. Rock, P. Carriere, P. Frigola, D. Gamzina, T. Horn, Characteristics and Processing of Hydrogen-Treated Copper Powders for EB-PBF Additive Manufacturing, Appl. Sci. 2019, Vol. 9, Page 3993. 9 (2019) 3993. https://doi.org/10.3390/APP9193993.

[37] P. Sun, Z.Z. Fang, Y. Zhang, Y. Xia, Review of the Methods for Production of Spherical Ti and Ti Alloy Powder, JOM. 69 (2017) 1853–1860, https://doi.org/10.1007/s11837-017-2513-5.

[38] H. Luo, P. Yu, G. Li, K. Yan, Topological quantum materials for energy conversion and storage, Nat. Rev. Phys. 2022 49. 4 (2022) 611–624. https://doi.org/10.1038/s42254-022-00477-9.

[39] M.H. Sehhat, A.T. Sutton, C.-H. Hung, B. Brown, R.J. O'Malley, J. Park, M.C. Leu, Plasma spheroidization of gas-atomized 304L stainless steel powder for laser

powder bed fusion process, Mater. Sci. Add. Manuf. 1 (1) (2022) 1, https://doi.org/10.18063/msam.v1i1.1.
[40] M.H. Sehhat, A.T. Sutton, C.-H. Hung, J.W. Newkirk, M.C. Leu, Investigation of Mechanical Properties of Parts Fabricated with Gas- and Water-Atomized 304L Stainless Steel Powder in the Laser Powder Bed Fusion Process, JOM 2021 (2021) 1–8, https://doi.org/10.1007/S11837-021-05029-7.
[41] T. Liu, C.S. Lough, H. Sehhat, Y. Ming, P.D. Christofides, E.C. Kinzel, M.C. Leu, In-situ infrared thermographic inspection for local powder layer thickness measurement in laser powder bed fusion, Addit. Manuf. 55 (2022), https://doi.org/10.1016/j.addma.2022.102873.
[42] Y. Xia, Z.Z. Fang, P. Sun, Y. Zhang, J. Zhu, Novel Method for Making Biomedical Segregation-Free Ti-30Ta Alloy Spherical Powder for Additive Manufacturing, JOM. 70 (2018) 364–369, https://doi.org/10.1007/S11837-017-2713-Z.
[43] M.H. Sehhat, J. Chandler, Z. Yates, A review on ICP powder plasma spheroidization process parameters, Int. J. Refract. Met. Hard Mater. 103 (2022) 105764, https://doi.org/10.1016/J.IJRMHM.2021.105764.
[44] Sehhat, M. Sutton, Austin, Leu, Ming. Enhancement of Gas-Atomized 304L Stainless Steel Powder by Plasma Spheroidization for use in the Laser Powder Bed Fusion Process. United States: N. p., (2022). Web. doi:10.2172/1876883.
[45] Z. Hao, Z. Fu, J. Liu, X. Zhu, F. Zhou, Y. Shu, J. Yi, J. He, Spheroidization of a granulated molybdenum powder by radio frequency inductively coupled plasma, Int. J. Refract. Met. Hard Mater. 82 (2019) 15–22, https://doi.org/10.1016/J.IJRMHM.2019.03.023.
[46] H. Zhu, H. Tong, C. Cheng, N. Liu, Study on behaviors of tungsten powders in radio frequency thermal plasma, Int. J. Refract. Met. Hard Mater. 66 (2017) 76–82, https://doi.org/10.1016/J.IJRMHM.2017.01.017.
[47] L. Vanel, A.D. Rosato, R.N. Dave, Rise-Time Regimes of a Large Sphere in Vibrated Bulk Solids, Phys. Rev. Lett. 78 (1997) 1255, https://doi.org/10.1103/PhysRevLett.78.1255.
[48] L. Labous, A.D. Rosato, R.N. Dave, Measurements of collisional properties of spheres using high-speed video analysis, Phys. Rev. E. 56 (1997) 5717, https://doi.org/10.1103/PhysRevE.56.5717.
[49] B. Li, H. Jin, F. Ding, L. Bai, F. Yuan, Fabrication of homogeneous Mo-Cu composites using spherical molybdenum powders prepared by thermal plasma spheroidization process, Int. J. Refract. Met. Hard Mater. 73 (2018) 13–21, https://doi.org/10.1016/J.IJRMHM.2018.01.022.
[50] H. Bissett, I.J. Van Der Walt, J.L. Havenga, J.T. Nel, Titanium and zirconium metal powder spheroidization by thermal plasma processes, J. South. African Inst. Min. Metall. 115 (2015) 937–942, https://doi.org/10.17159/2411-9717/2015/v115n10a6.
[51] N.J.M. Grobler, H. Bissett, G.J. Puts, P.L. Crouse, Finite-element analysis of the effect of sheath-gas composition in an inductively-coupled plasma, IOP Conf. Ser. Mater. Sci. Eng. 430 (2018), https://doi.org/10.1088/1757-899X/430/1/012024.
[52] Y. Siregar, Y. Tanaka, T. Ishijima, Y. Uesugi, Influence of sheath gas flow rate in Ar induction thermal plasma with Ti powder injection on the plasma temperature by numerical calculation, MATEC Web Conf. 218 (2018) 04030, https://doi.org/10.1051/MATECCONF/201821804030.